New Materials, Compounds and Applications
Vol.7, No.2, 2023, pp.76-83

AN UPDATE PHASE DIAGRAM OF THE Sb_2Te_3-Sb_2S_3 SYSTEM

F.R. Aliyev[1*], E.N. Orujlu[1], G.B. Dashdiyeva[2,3], A.L. Mustafayeva[3], D.M. Babanly[1,4]

[1]Azerbaijan State Oil and Industry University, French – Azerbaijani University, Baku, Azerbaijan
[2]Baku Engineering University, Baku, Azerbaijan
[3]Baku State University, Baku, Azerbaijan
[4]Institute of Catalysis and Inorganic Chemistry (ICIC), Ministry of Science and Education of the Republic of Azerbaijan, Azerbaijan

Abstract. Updated phase diagram of the Sb_2Te_3-Sb_2S_3 system was constructed using X-ray diffraction analysis (XRD), differential thermal analysis (DTA), scanning electron microscopy (SEM), and energy dispersive spectroscopy (EDS) methods. In previous studies, this phase diagram was characterized as eutectic type without any intermediate compound. In this work, we report the existence of a tetradymite-like compound Sb_2Te_2S, which melts with decomposition by a peritectic reaction at 758 K. Based on XRD analysis, this compound crystallizes in a tetradymite-type hexagonal structure and has following lattice parameters: a = 4.1675 Å, c = 29.483 Å.

Keywords: *Sb_2Te_3-Sb_2S_3 system, phase diagram, tetradymite-like structure, topological insulators.*

Corresponding Author: *Fariz Aliyev, Azerbaijan State Oil and Industry University, French -Azerbaijani University, Nizami str. 183, Baku, Azerbaijan, e-mail: fariz_ar@hotmail.com*

Received: *7 May 2023;* ***Accepted:*** *27 June 2023;* ***Published:*** *4 August 2023.*

1. Introduction

Chalcogenide-based heavy p-block elements have been known as the world's best thermoelectrics (TEs) for room-temperature operation (Yixuan *et al*., 2019; Taishan *et al.*, 2021; Teng *et al*., 2020; Kwork *et al.*, 2019; Yuan *et al*., 2019). Also, such materials are the main constituent in the design of energy conversion devices, solar panels, infrared detectors, new-generation refrigerators, semiconductors, etc. (Hong *et al.*, 2022; He *et al.*, 2016; Ahluwalia *et al.*, 2017; Xia *et al.*, 2016; Youngjun *et al.*, 2021). In the last decade, the discovery of a new quantum state of matter - a three-dimensional topological insulator (TI) (Joel, 2010; Rachel *et al.*, 2018) shows the unique transport properties of electrons in a topological surface state (TSS). This has drawn a lot of attention to binary (Caterina *et al.*, 2016a,b; Conor *et al.*, 2019; Marco *et al.*, 2016; Flamminil *et al.*, 2018) and more complex (Pacilè *et al.*, 2018; Estyunin *et al.*, 2020; Shikin *et al.*, 2020; Ilya *et al.*, 2020; Munisa *et al.*, 2020) layered narrow-gap semiconductors. It was found that layered phases with TIs properties are considered extremely promising for various applications including spintronic, medicine, quantum computers, lasers, security systems, etc. (Babanly *et al.*,

How to cite (APA):
Aliyev, F.R., Orujlu, E.N., Dashdiyeva, G.B., Mustafayeva, A.L., & Babanly, D.M. (2023). An update phase diagram of the Sb_2Te_3-Sb_2S_3 system. *New Materials, Compounds and Applications, 7*(2), 76-83.

2017; He *et al.,* 2019; Rabia *et al.,* 2018; Orujlu *et al.,* 2022; Wenchao *et al.,* 2017; Hua *et al.,* 2019).

The tetradymite mineral- Bi_2Te_2S which exhibits interesting thermoelectric and optical properties has binary and ternary structural analogs (Tao *et al.,* 2021; Ryu *et al.,* 2019; Annese *et al.,* 2018). The binary chalcogenides of tetradymite-type structures have chalcogen atoms in their crystal structures that occupy two positions and differ from each other by coordination, which is either an octahedron or pyramid. In these types of compounds each five-layer slab consists of alternating monoatomic hexagonal layers. Neighboring stacks are bonded by Van der Waals forces, allowing crystals to be readily cleaved by planes. It is for this reason that tetradymite compounds are classified with layered materials (Babanly *et al.,* 2017)

A new phase Sb_2Te_2S (Grauner *et al.,* 2019) with a tetradymite structure, which is located in the Sb_2Te_3-Sb_2S_3 system have been discovered recently. The literature contains only a limited amount of information about the phase diagram of this system (Jafarov *et al.,* 2014). In mentioned work, the Sb_2Te_2S ternary compound was not detected in the phase diagram of the Sb_2Te_3-Sb_2S_3 system and it was shown that this phase diagram is of an eutectic type.

Hence, the purpose of this work is to obtain a new refined picture of phase equilibria in the Sb_2Te_3-Sb_2S_3 system.

The primary compounds of the system have been studied in detail. It has been established that the Sb_2Te_3 compound melts congruently at 895 K (Solé *et al.,* 2022). This compound has a rhombohedral lattice (sp.gr. R-3m) of the tetradymite type with the following lattice parameters in the hexagonal configuration: a=4.264 Å, c=30.458 Å (Anderson *et al.,* 1974). The Sb_2S_3 compound also melts congruently at 819K (Massalski *et al.,* 1990) and crystallizes in the orthorhombic structure and belongs to the space group Pnma with the following lattice parameters a = 11.3107 Å, b = 3.8363 Å, and c = 11.2285 Å (Bayliss *et al.,* 1972).

2. Experimental part

The initial compounds were synthesized by melting high purity Sb, Te, and S elements (99.999%, Alfa Aesar) in quartz ampoules under vacuum (10^{-2} Pa). The Sb_2Te_3 compound was synthesized in a single zone furnace at 900 K. The Sb_2S_3 compound was synthesized in a two-zone furnace (due to the high sulfur vapor pressure). The temperature of the "cold" zone was 650 K, which is below the boiling point of sulfur (718 K (Emsley *et al.,* 1998), while the temperature of the "hot" zone was maintained 30–50 K above the melting point of Sb_2S_3. The synthesis was continued in this mode for 3-4 hours, after the disappearance of sulfur vapor in the "cold" zone, the ampoule was completely transferred to the hot zone. After stirring the homogeneous liquid in the ampoule, the oven was gradually cooled down. Then the ampoule was annealed at 600 K for 300 hours. Obtained results of diffraction patterns of primary compounds are in good agreement with the literature data (Fig. 1) (Arun *et al.,* 1996; Indu *et al.,* 2019).

Samples of various compositions (0.5 g each) of the Sb_2Te_3-Sb_2S_3 system were synthesized in evacuated quartz ampoules and then were annealed at 600K for 500 hours to reach an equilibrium state.

The synthesized ingots were studied by X-ray phase analysis at room temperature in the range of 2θ = 5-75 degrees on a Bruker D2 PHASER X-ray diffractometer using $CuK_{\alpha 1}$ radiation. The lattice parameters were calculated using the TOPAS V4.2 program.

A NETZSCH 404 F1 Pegasus system was used for differential thermal analysis. The DTA of the annealed alloy was carried out from room temperature to 900 K with a heating and cooling rate of 10 K min^{-1}. For SEM analyses used Tescan Vega 3 SBH Scanning Electron Microscope device. The energy dispersive X-ray spectroscopy (EDX) method used for elemental analysis of synthesized ingots.

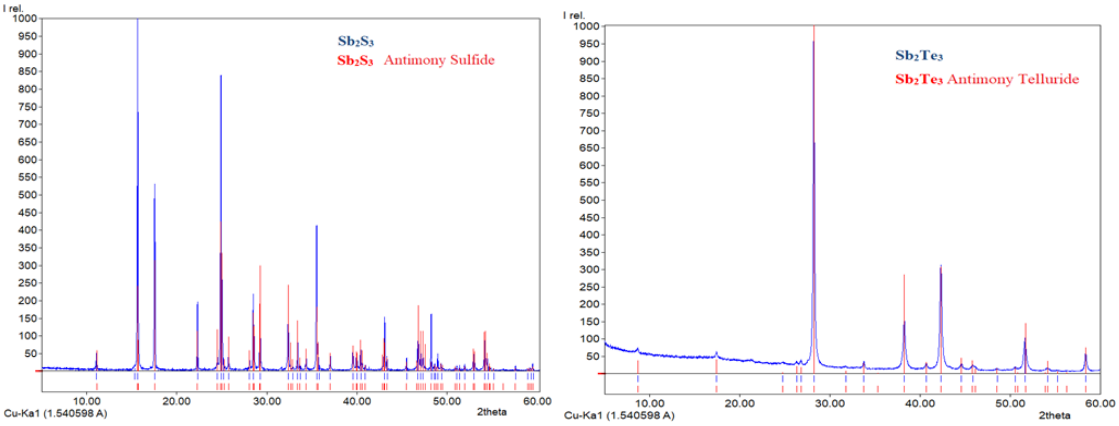

Fig. 1. XRD pattern of the a) Sb_2S_3 (Arun *et al.*, 1996); b) Sb_2Te_3 (Indu *et al.*, 2019)

3. Results and discussion

Fig. 2 shows X-ray diffraction patterns of thermally treated alloys. As can be seen, diffraction patterns of Sb_2S_3 and 10 mol % Sb_2Te_3 composition are similar to each other and differs only by a slight shift of the diffraction lines to smaller angles.

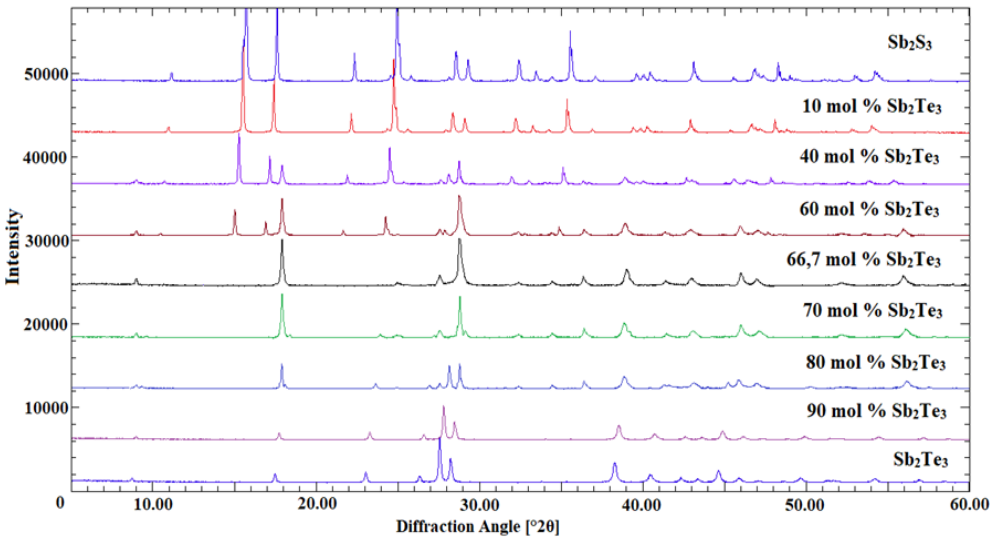

Fig. 2. XRD patterns for different alloys of the Sb_2S_3 – Sb_2Te_3 system

Similarly, the diffraction pattern of the 90 mol % Sb_2Te_3 sample consists mainly of the Sb_2Te_3 diffraction peaks of the solid solution based on Sb_2Te_3. Diffraction patterns of the samples containing 40, 60, 70, and 80 mol % Sb_2Te_3 show their non-homogeneity possessing diffraction lines of two different phases where one of them is Sb_2Te_2S (γ phase). In diffraction patterns of the 40 and 60 mol % Sb_2Te_3 alloys, besides γ phase there

is also diffraction peaks of α phase based on Sb_2S_3. Analysis of the XRD pattern of the 66.7 mol % Sb_2Te_3 stoichiometric composition indicates the existence of a ternary compound without any traces of other phases with the unit cell parameters: a = 4,1675 Å, c = 29,483 Å.

Since there are no diffraction lines of the Sb_2Te_2S compound in the database, Fig. 3 shows the diffraction pattern of the alloy of this phase compared to the Bi_2Te_2S compound. As can be seen, the Sb_2Te_2S compound has a diffraction pattern characteristic of the tetradymite structure, and the diffraction peaks are slightly shifted towards larger angles compared to the Bi_2Te_2S compound. The lattice parameters obtained by us (a = 4.1675 Å; c = 29.483 Å) are in a good agreement with (Grauner *et al.*, 2019).

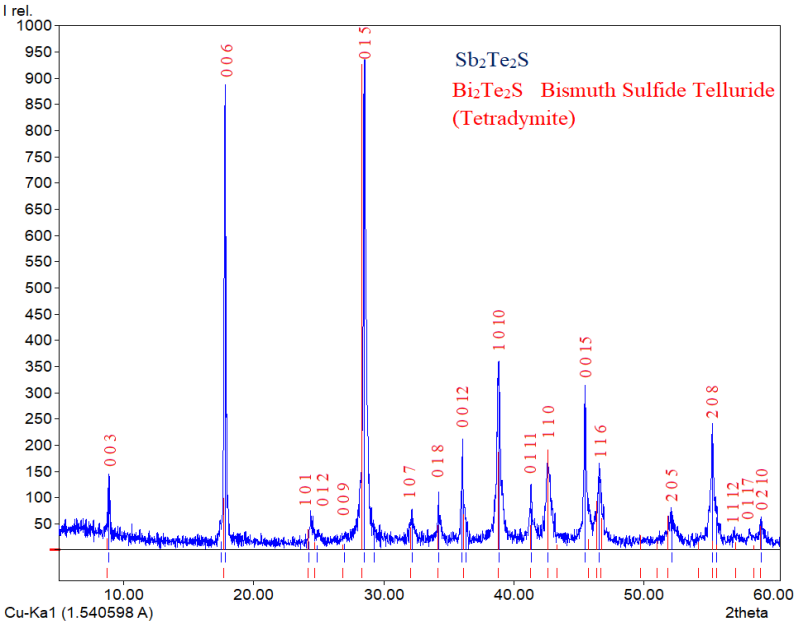

Fig. 3. XRD pattern of the Sb_2Te_2S

The phase diagram of the Sb_2S_3 – Sb_2Te_3 system was constructed based on the DTA and XRD results of annealed alloys. During thermal analysis, an additional thermal effect at 748 K was observed on the DTA heating curve of the Sb_2Te_2S alloy (Fig.4a). This shows that the alloy is in a non-equilibrium state. To continue with, the alloy was additionally ground into powder, pressed into a tablet and then was subjected to an additional annealing at 600 K for 500 h. After subsequent thermal analysis, on the thermogram of the same sample the thermal effect at 748 K completely disappears while the intensity of the peak at 758 K increases significantly (Fig. 4b). The last peak at 845 K indicates the liquidus temperature.

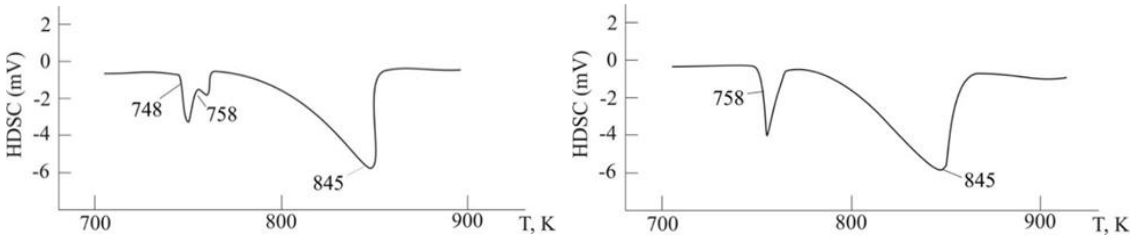

Fig. 4. DTA heating thermograms of the: a) Sb_2Te_2S b) additionally annealed Sb_2Te_2S

The phase diagram of the Sb_2S_3 – Sb_2Te_3 system is given in the Fig. 5. As can be seen from the figure, in this quasi-binary system, there is only one ternary compound that melts at 758 K according to the peritectic reaction:

$$L + Sb_2Te_3(\beta) \leftrightarrow Sb_2Te_2S$$

The composition of the invariant peritectic point corresponds to 23 mol % (p) Sb_2Te_3.

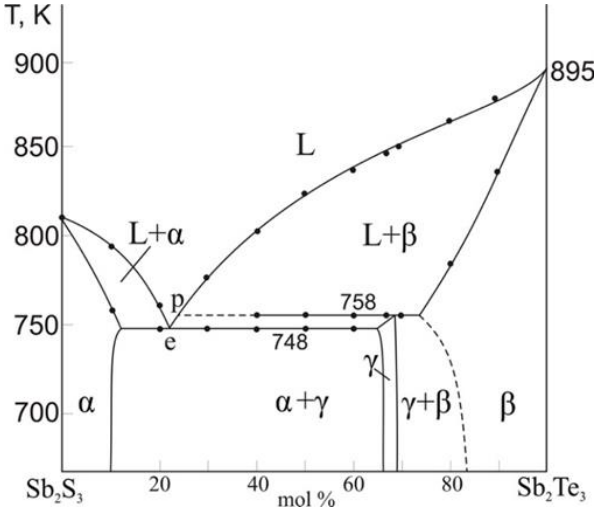

Fig. 5. Phase diagram of the Sb_2S_3 – Sb_2Te_3 system

The system also has an eutectic point (e) which lies at 21 mol % Sb_2Te_3 and 748 K. Ternary Sb_2Te_2S has a very narrow primary crystallization area meaning that it is extremely difficult to obtain a phase-pure crystalline sample due to direct synthesis. This phase has a significant homogeneity area (γ phase) approximately from 66,7 to 69 mol % Sb_2Te_3. The system has two bi-phasic areas based on the initial and ternary compounds. The bi-phasic area based on Sb_2S_3 (α phase) was detected from ~10 to 66,7 mol % Sb_2Te_3 and the second one based on Sb_2Te_3 (β phase) was detected from ~69 to 83 mol % Sb_2Te_3. It is worth mentioning that the updated phase diagram for the Sb_2S_3 – Sb_2Te_3 system differs from the available version (Jafarov *et al.,* 2014) in regard of detection a new ternary compound.

Fig. 6. SEM images of the alloy containing 66.7 mol. % Sb_2Te_3

Table 1. Elemental microanalysis results of the 66.7 mol. % Sb_2Te_3 sample

Element	Weight %	Atom %	Error %
Antimony	46.98	41.54	1.37
Tellurium	47.75	41.83	1.84
Sulphur	5.27	16.63	3.17
	100	100	

The SEM image of a sample with 66.7 mol. % Sb_2Te_3 composition is shown in the Fig. 6. The image confirms that the sample is single-phase and has a layered structure. The results of elemental microanalysis by the EDS method of the same sample are shown in Table 1. As can be seen, the elemental composition corresponds to the stoichiometry of this alloy.

4. Conclusion

Based on the results of the DTA, XRD, SEM and EDS methods, a new phase diagram of the Sb_2Te_3-Sb_2S_3 system was constructed, which differs from the previous one. The updated phase diagram is characterized by the formation of layered tetradymite-like ternary compound Sb_2Te_2S, which melts by decomposition at 758 K. A very narrow primary crystallization field and 2 bi-phasic regions based on the initial phases and the ternary compound were found at the system. The X-ray diffraction pattern shows that the Sb_2Te_2S ternary compound has crystal lattice parameters a = 4.1675 Å, c = 29.483 Å. This ternary phase has a practical interest as a potential thermoelectric and topological insulator material.

References

Ahluwalia, G.K. (2017). Fundamentals of Chalcogenides in Crystalline, Amorphous, and Nanocrystalline Forms. In *Applications of chalcogenides: S, Se, and Te*. Springer, Cham. https://doi.org/10.1007/978-3-319-41190-3_1

Anderson, T.L., Krause, H.B. (1974). Refinement of the Sb_2Te_3 and Sb_2Te_2Se structures and their relationship to nonstoichiometric Sb_2Te_3− ySey compounds. *Acta Crystallographica Section B: Structural Crystallography and Crystal Chemistry*, *30*(5), 1307-1310.

Annese, E, Okuda T., Schwier, E. F., Iwasawa, H., Shimada, K., Natamane, M., Taniguchi, M., Rusinov, I.P., Eremeev, S.V., Kokh, K.A., Golyashov, V.A., Tereshchenko, O.E., Chulkov, E.V., & Kimura, A. (2018). Electronic and spin structure of the wide-band-gap topological insulator: Nearly stoichiometric Bi_2Te_2S. *Physical Review B.*, *97*(20), 205113.

Arun, P., Vedeshwar, A.G. (1996). On the structure of stibnite (Sb_2S_3). *Journal of Materials Science*, 31, 6507-6510.

Babanly, M.B., Chulkov, E.V., Aliev, Z.S., Shevelkov, A.V., & Amiraslanov, I.R. (2017). Phase diagrams in materials science of topological insulators based on metal chalcogenides. *Russ. J. Inorg. Chem.*, *62*(13), 1703–1729.

Bayliss, P., Werner, N. (1972). Refinement of the crystal structure of stibnite, Sb_2S_3. *Zeitschrift für Kristallographie-Crystalline Materials*, *135*(1-6), 308-315.

Caterina, L., Anna, C., Antonio, P., Ziya, S.A., Mahammad, B.B., Evgueni, V.C., Marco, A., & Leonardo, P. (2016a). Nanoindentation of single-crystal Bi_2Te_3 topological insulators grown with the Bridgman–Stockbarger method. *Physica Status Solidi (B)*, *254*(6), 1082-1086.

Caterina, L., Anna, C., Antonio, P., Ziya, S.A., Mahammad, B.B., Evgueni, V.C., & Leonardo, P. (2016b). Indentation fracture toughness of single-crystal Bi_2Te_3 topological insulators. *Nano Research*, 9, 1032-1042.

Conor, H., Kris, H., Fabio, R., Stefano, C., Simone, S., Paolo, M., Polina, M.S., Sanjoy, M., Marco, P., Ziya, S.A., Mahammad, B., Evgeni, V.C., Carlo, C., & Roberto, F. (2019). Temperature driven phase transition at the antimonene/Bi_2Se_3 van der Waals heterostructure. *ACS nano, 13*(9), 10481-10489.

Emsley, J. (1998). *The Elements.* New York: Oxford University Press, 3rd ed., 300.

Estyunin, D.A., Klimovskikh, I.I., Shikin, A.M., Schwier, E.F., Otrokov, M.M., Kimura, A., Kumar, S., Filnov, S.O., Aliev, Z.S., Babanly, M.B., & Chulkov, E.V. (2020). Signatures of temperature driven antiferromagnetic transition in the electronic structure of topological insulator $MnBi_2Te_4$. *APL Materials, 8*(2), 021105.

Flammini1, R., Colonna, S., Hogan, C., Mahatha, S.K., Papagno, M., Barla, A., Sheverdyaeva, P.M., Moras, P., Aliev, Z.S., Babanly, M.B., & Chulkov, E.V. (2018). Evidence of β-antimonene at the Sb/Bi_2Se_3 interface. *Nanotechnology*, *29*(6), 065704.

Grauer, D.C., Hor, Y.S., Williams, A.J., & Cava, R.J. (2009). Thermoelectric properties of the tetradymite-type Bi_2Te_2S–Sb_2Te_2S solid solution. *Materials Research Bulletin, 44*(9), 1926-1929.

He, T., Matthew, L.C., Sina, N., Qiushi, G., Fengnian, X., & Madan D. (2016). Optoelectronic devices based on two-dimensional transition metal dichalcogenides. *Nano Research*, 9, 1543–1560.

He, M., Huimin, S., & Qing, L.H. (2019). Topological insulator: Spintronics and quantum computations. *Frontiers of Physics*, 14, 1-16.

Hua, L., Siqing, D., Zengji, Y., Yicun, F., Huachao, C., Jianglei, D., Dong, M., Enpu, L., Ting, M., & Jianlin, Z. (2019). Sb_2Te_3 topological insulator: surface plasmon resonance and application in refractive index monitoring. *Nanoscale, 11*(11), 4759-4766.

Hong, C., Mao-Yin, R., Wen-Bo, W., & Qi-Long, Z. (2022) A comprehensive review on metal chalcogenides with three-dimensional frameworks for infrared nonlinear optical applications. *Coordination Chemistry Reviews*, 470, 214706.

Ilya, I., Klimovskikh, M.M., Otrokov, D., Estyunin, S.V., Eremeev, S.O., Filnov, A.K., Eugene S., Vladimir V., Artem G.R., Igor P.R., Maria B.R., Martin H., Ziya S.A., Mahammad B.B., Imamaddin R.A., & Nadir A.A.(2020). Tunable 3D/2D magnetism in the $(MnBi_2Te_4)(Bi_2Te_3)_m$ topological insulators family. *NPJ Quantum Materials*, *5*(1), 54.

Jafarov, Y.I., Babanly, M.B., Amiraslanov, I.R., Gasimov, V.A., Shevelkov, A.V., & Aliev, Z.S. (2014). Study of the $3Tl_2S + Sb_2Te_3 \leftrightarrow 3Tl_2Te + Sb_2S_3$ reciprocal system. *Journal of Alloys and Compounds*, 582, 659-669.

Joel, M. (2010). The birth of topological insulators. *Nature*, 464, 194–198.

Youngjun, K., Whang, J.W., Donghyun K., Sangyoon L., Seung-min C., Jusang P., & Hyungjun K. (2021). Atomic-Layer-Deposition-Based 2D Transition Metal Chalcogenides: Synthesis, Modulation, and Applications. *Advanced Materials*, *33*(47), 2005907.

Kwok, W.S, Su-Xi, W., Yun, Z., & Jianwei, X. (2019). Solution-Based Synthesis and Processing of Metal Chalcogenides for Thermoelectric Applications. *Applied Sciences*, *9*(7), 1511.

Marco, C., Mirko, P., Simone, L., Lama, K., Giovanni, D.S., Evangelos, P., Andrzej, H., Marcin, K., Lia, K.E., Ziya, S.A., Mahammad, B.B., & Mikhail, M.O. (2016). Manipulating the topological interface by molecular adsorbates: adsorption of Co-phthalocyanine on Bi_2Se_3. *Nano Letters*, *16*(6), 3409-3414.

Massalski, T.B., Murray, J.L., & Bennett, L.H. (1990). Binary alloy phase diagrams Materials park. *ASM International, Materials Park, OH, USA*, 12.

Munisa, N., Kazuaki, O., Siyuan, Z., Tatiana, V.M., Igor, P.R., Vladislav, O.K., Koji, Miyamoto, Taichi, O., Takeo, M., Xiaoxiao, W., Yukiaki, I., Kazuki, S., Eike, F., Schwier, M.Y., Ziya, S., Mahammad, B. B., Imamaddin, R.A., & Evgueni, V.C. (2020). Topologically nontrivial phase-change compound $GeSb_2Te_4$. *ACS Nano, 14*(7), 9059-9065.

Orujlu, E., Aliev, Z., & Babanly, M. (2022). The phase diagram of the MnTe–SnTe– Sb_2Te_3 ternary system and synthesis of the iso and aliovalent cation-substituted solid solutions. *Calphad*, 76, 102398.

Pacilè, D., Eremeev, S.V., Caputo, M., Pisarra, M., De L., Grimaldi, O., Fujii, I., Aliev, Z.S., Babanly, M.B., Vobornik, I., Agostino, R.G., Goldoni, A., Chulkov, E.V., & Papagno, M. (2018). Deep insight into the electronic structure of ternary topological insulators: A comparative study of $PbBi_4Te_7$ and $PbBi_6Te_{10}$. *physica status solidi (RRL)–Rapid Research Letters*, *12*(12), 1800341.

Indu, R., Sumesh, R., Rudra, P.J., & Archana, L. (2019). Crystal growth and x-ray diffraction characterization of Sb_2Te_3 single crystal. *AIP Conference Proceedings AIP Publishing LLC.*, *2100*(1), 020070.

Rabia, S., Ganesh, G., Patnaik, S., & Awana, V. (2018). Crystal growth and characterization of bulk Sb_2Te_3 topological insulator. *Materials Research Express*, *5*(4), 46107.

Rachel, S. (2018). Interacting topological insulators: a review. *Reports on Progress in Physics*, *81*(11), 116501.

Ryu, B., Ji, L., Ji, E., & Son, H. (2019). Highly anisotropic thermoelectric transport properties responsible for enhanced thermoelectric performance in the hot deformed tetradymite Bi_2Te_2S. *Journal of Alloys and Compounds*, 783, 448– 454.

Shikin, A.M., Estyunin, D.A., Klimovskikh, I.I., Filnov, S.O., Schwier E.F., Kumar, S., Miyamoto, K., Okuda, T., Kimura, A., Kuroda, K., Yaji, K., Shin, S., Takeda, Y., Saitoh Y., Aliev, Z.S., Mamedov, N. T., Amiraslanov, I.R., Babanly, M.B., Otrokov, M.M., Eremeev, S.V., & Chulkov, E.V. (2020). Nature of the Dirac gap modulation and surface magnetic interaction in axion antiferromagnetic topological insulator $MnBi_2Te_4$. *Scientific Reports*, *10*(1), 13226.

Solé, S., Clemens S., & Klaus, W.R. (2022). A Revision of the Sb-Te Binary Phase Diagram and Crystal Structure of the Modulated γ-Phase Field. *Journal of Phase Equilibria and Diffusion*, 43, 648-659.

Taishan, Z., Ran, H., Sheng, G., Kornelius, N., & Jeffrey, C. (2021). Charting lattice thermal conductivity for inorganic crystals and discovering rare earth chalcogenides for thermoelectrics. *Energy Environ. Sci*., 14, 3559-3566.

Tao, Q., Fanchen, M., Zhengkai, Z., Yu, C., Yingdei, T., Jinggeng, Z., Xianli, S., Ctirad, U., & Xinfeng, T. (2021). The origin of ultra-low thermal conductivity of the Bi_2Te_2S compound and boosting the thermoelectric performance via carrier engineering. *Materials Today Physics*, 20, 100472.

Teng, W., Taichang, H., Hongchao, W., & Chunlei, W. (2020) Quaternary chalcogenides: Promising thermoelectric material and recent progress. *Sci China Mater.*, *63*(1), 8–15.

Xia, C., & Jingbo, Li. 2016. Recent advances in optoelectronic properties and applications of two-dimensional metal chalcogenides. *Journal of Semiconductors*, *37*(5), 051001.

Yixuan, S., Cheryl, S., & Holger, K. (2019). Chalcogenides as thermoelectric materials. *Journal of Solid State Chemistry*, 270, 273-279.

Yuan, Y., Matteo, C., Oana, C., & Matthias, W. (2019). Chalcogenide Thermoelectrics Empowered by an Unconventional Bonding Mechanism. *Advanced Functional Materials*, *30*(8), 1904862.

Wenchao T., Wenbo, Y., Jing S., & Yongkun, W. (2017). The property, preparation and application of topological insulators: a review. *Materials*, *10*(7), 814.